Catalysis Today xxx (2016) xxx–xxx

Contents lists available at ScienceDirect

Catalysis Today

journal homepage: www.elsevier.com/locate/cattod

Selective hydrogenolysis of glycerol over Ir-Ni bimetallic catalysts

Aracelis J. Pamphile-Adrián[a], Pedro P. Florez-Rodriguez[a], Mattheus Henrique M. Pires[a], Geronimo Perez[b], Fabio B. Passos[a,*]

[a] Departamento de Engenharia Química e de Petróleo, Universidade Federal Fluminense, Rua Passos da Pátria, 156, 24210-040, Niterói, RJ, Brazil
[b] Instituto Nacional de Metrologia (INMETRO), Divisão de Metrologia de Materiais (DIMAT), Av. Nossa Senhora das Graças, 50, 25250-020, Xerém, Duque de Caxias, RJ, Brazil

ARTICLE INFO

Article history:
Received 15 May 2016
Received in revised form 9 July 2016
Accepted 27 July 2016
Available online xxx

Keywords:
Glycerol hydrogenolysis
Iridium catalyst
Bimetallic catalysts
Nickel catalyst
Biodiesel

ABSTRACT

The effect of the addition of Ni to Ir/γ-Al_2O_3 was studied for glycerol hydrogenolysis reaction. The catalysts were characterized by textural analysis, XRD, H_2-TPR, XPS and TEM. In all cases, the addition of Ni to Ir/γ-Al_2O_3 produced a significant increase in glycerol conversion, and a high selectivity to 1,2-PDO was maintained. TOF values increased from 0.4×10^{-2} s^{-1} for Ir monometallic catalyst, to 4.3×10^{-2} s^{-1} for bimetallic $IrNi_2$_C catalyst. The latter was the most active catalyst among the calcined bimetallic catalysts. Selectivity to 1,2-PDO had an insignificant decrease from 89.9% for Ir monometallic catalyst to 83.1% for $IrNi_2$_C catalyst. However, non-calcined $IrNi_2$ catalyst presented a TOF value of 1.3×10^{-2} s^{-1}. This result indicates that the calcination step was fundamental to obtain a strong Ir-Ni interaction that lead to better performances of the bimetallic catalysts. Ir-Ni interaction was evidenced by XPS analyses of the calcined series of catalysts, where the presence of an $Ir^{\delta+}$ species was observed ($0 < \delta < 4$), suggesting an electronic density transferring from Ni to Ir.

1. Introduction

The investigation of renewable energy alternatives has been an important concern recently and has led to the exploration of biodiesel as an alternative to fossil fuels. Biodiesel is obtained from fat oils by the transesterification with an alcohol [1], and crude glycerol is obtained as a by-product [2]. In this context, the search for synthesis routes aiming the transformation of glycerol into high value products has grown in the last years. Catalytic hydrogenolysis is an interesting route for obtaining high value materials such as 1,2-propanediol (1,2-PDO), 1,3-propanediol (1,3-PDO), and other alcohols.

Different supported noble and non-noble metal catalysts have been employed for the selective hydrogenolysis of glycerol. Low activity for hydrogenolysis of glycerol with supported iridium catalysts have been reported [3–6]. Nakagawa et al. [3] reported a low conversion of glycerol for a 4% Ir/SiO_2 catalyst, however, a great increase in activity and selectivity for 1,3-PDO was observed when the catalyst was promoted with ReO_x. Ir-ReO_x/SiO_2 catalyst presented about 90% of glycerol conversion after 48 h of reaction and a maximum yield of 1,3-PDO of 38% at 36 h of reaction. Based in the results of this work, the authors proposed a reaction mechanism that involves the glycerol adsorption on the ReO_x cluster and the attack of an activated hydrogen on metallic Ir to explain the formation of 1,3-propanediol. Subsequently, other investigations have been developed by this research group to elucidate the effect of reaction parameters like Re/Ir rate, type of acid co-catalyst, as well as determining the structure of Ir-ReO_x/SiO_2 catalyst and the effect of the addition of Ru as a promoter [7–10]. Furtheremore, the activity of this bifunctional catalyst have been studied for C—O bonds hydrogenolysis of different biomass derived substrates using solvents as water and alkanes [11,12]. The activity of the catalyst was strongly depedent of the solvent used. Alkane solvent was advantageous on water in the hydrogenolysis of secondary mono-alcohols due the stronger adsorption of the substrate on the catalyst surface, leading to a two-setep indirect mechanism (acid-catalyzed dehydration and subsequent hydrogenation) [11]. In the presence of water, hydrogenolysis was promoted by the addition of acid cocatalysts, which was explained by the promoter effect of Re alkoxide formation under an acidic atmosphere, leading to the C—O bond hydrogenolysis by direct mechanism [12].

Recently, other properties of Ir-Re catalysts have been studied as suport [13] and structural [14,15] effects. It was found that Ir-Re supported on alumina-silica material (ASA) was nearly inactive,

* Corresponding author.
E-mail addresses: aracelispamphile@id.uff.br (A.J. Pamphile-Adrián), pedropablofr@gmail.com (P.P. Florez-Rodriguez), mhenrique_mp@hotmail.com (M.H.M. Pires), perezgeronimo@hotmail.com (G. Perez), fbpassos@vm.uff.br, fabiopassos@id.uff.br (F.B. Passos).

http://dx.doi.org/10.1016/j.cattod.2016.07.026
0920-5861/

which was attributed to the strong Re-support interaction that promotes the dispersion of Re species, difficulting the sinegy between Ir and Re. However, Ir-Re supported on de-aluminated ASA (ASA treated with 0.05 or 0.5 M HNO_3) showed an enhanced activity and selectivity to 1,3-PDO, as a result of the formation of active Ir-Re alloy nanoparticles [13]. This Ir-Re alloy was shown to be more active than Ir-ReOx structure (both supported on mesoporous silica KIT-6). Besides the enhanced activity, Ir-Re alloy presented double 1,3-PDO formation rate, and enhanced resistance against particle sintering [14].

Previously, we have studied the activity and selectivity of Al_2O_3, SiO_2 and ZrO_2 supported iridium catalysts in C—C and C—O cleavage in cyclohexane conversion and glycerol hydrogenolysis [16]. The effect of support, H_2 initial pressure and temperature reaction on glycerol conversion and products selectivity were explored. When reaction was performed at 200 °C, glycerol conversion was 8.3% for Ir/ZrO_2 catalyst, 7.7% for Ir/γ-Al_2O_3 catalyst and 3.9% for Ir/SiO_2 catalyst, and a maximum selectivity for 1,2-PDO of 86.7% was obtained with Ir/SiO_2 catalyst. For a higher reaction temperature (250 °C), higher values of conversion were obtained, however, a decrease in selectivity to 1,2-PDO was also observed. At this temperature, several undesired products as short and long chain alcohols, ketones, esters, ethers and aldehydes were formed. The results showed that both C—O and C—C hydrogenolysis were influenced by acidic properties of the support, the electronic state of the active phase and the different metal-support interactions [16]. Consequently, the present manuscript addresses the addition of Ni as a second metal to Ir/γ-Al_2O_3 aiming the increase of the catalyst activity with a high selectivity to 1,2-PDO. Mono- and bimetallic Ni based catalysts have shown activity for glycerol conversion reactions [17–19].

The performances of bimetallic Ni-Ir catalysts have been investigated in several reactions involving C—H cleavage like methane dissociation [20], and H_2 production by hydrated hydrazine decomposition [21] and partial oxidation of methane [22]. Additionally, the addition of Ir to TiO_2 supported Ni catalysts produced an activity increase in the cinnamaldehyde hydrogenation due the strong interaction between Ni and Ir that modified the electronic structure of the surface Ni [23]. A similar effect was obtained in the ammonia decomposition, where the addition of Ir to a Ni/γ-Al_2O_3 catalyst caused an increase of 40% in conversion, suggesting the presence of a synergic effect that reduces the interaction of the active phase with the support and favors the formation of more active sites [24]. On the other hand, the addition of Ni to Ir/γ-Al_2O_3 catalysts was shown to be efficient in suppressing substituted C—C cleavage in 1,3-dimethylcyclohexane ring opening, allowing the formation of products with better cetane number and moderate vapor pressure [25].

In this work, the effect of the addition of different amounts of Ni to an Ir/γ-Al_2O_3 catalyst for glycerol hydrogenolysis reaction was investigated. The effect of the Ir-Ni interactions on glycerol conversion and selectivity to 1,2-PDO was studied.

2. Experimental

2.1. Catalyst preparation

Commercial γ-Al_2O_3 (Puralox HP-14) calcined at 600 °C (5 °C/min during 4 h) was used. The monometallic iridium and nickel catalysts were prepared by incipient wetness impregnation technique, using solutions of $H_2IrCl_6{\cdot}xH_2O$ (Sigma-Aldrich) and $Ni(NO_3)_2{\cdot}9H_2O$, to yield 2 wt.% Ir and 3 wt.% Ni, respectively. "Ni_C" catalyst was obtained after drying of the impregnated solid at 100 °C for 16 h, and calcination at 500 °C during 4 h (10 °C/min). Iridium impregnated solid was dried at 70 °C for 16 h due the low melting point of the $H_2IrCl_6{\cdot}xH_2O$ (65 °C), this solid was denoted as "Ir" catalyst. Finally, "Ir_C" catalyst was prepared by calcination of "Ir" catalyst at 400 °C during 4 h (10 °C/min).

For bimetallic catalysts Ir content was maintained at 2 wt.%, and Ni content was adjusted for obtaining Ni/Ir = 0.5; 1.0 e 2.0 molar ratios.

For the preparation of these solids, first the support was impregnated with a $Ni(NO_3)_2{\cdot}6H_2O$ (Sigma-Aldrich) aqueous solution. Then, the precursors were dried at 100 °C during 16 h and calcined at 500 °C (10 °C/min) during 4 h. Finally, the solids were impregnated with an $H_2IrCl_6{\cdot}xH_2O$ (Sigma-Aldrich) aqueous solution, and the precursors were dried at 70 °C during 16 h. Finally, calcination of bimetallic catalyst was performed at 500 °C (10 °C/min) during 4 h.

Non-calcined and calcined solids ($IrNi_x$ and $IrNi_x$_C, respectively) were reduced and passivated in a fixed bed reactor prior to catalytic runs. The solids were dried at 150 °C for 30 min under He flow (30 mL/min) and cooled to room temperature. The reduction was performed at 500 °C in H_2 flow (30 mL/min) during 2 h, then catalysts were passivated with a 5% O_2/He flow at liquid N_2 temperature.

2.2. Catalyst characterization

Nitrogen adsorption isotherms of the samples were measured using a Micromeritics ASAP 2020 equipment. Surface areas were calculated using the Brunauer–Emmett–Teller (BET) equation. X-ray diffraction (XRD) experiments were performed using a Miniflex RIGAKU spectrometer (CuKα radiation). The diffractograms were obtained between $2\theta = 10°$ and 80° using a 0.02° step size (1 step/s).

Temperature programmed reduction (TPR) experiments were performed with a multipurpose unit coupled to a Prisma quadrupole mass spectrometer (Pfeiffer). The samples were dried at 150 °C for 30 min under He flow (30 mL/min) and cooled to room temperature, then the samples were submitted to a 5% H_2/Ar gas flow (30 mL/min) and the temperature was raised to 1000 °C at a heating rate of 10 °C/min.

CO chemisorption analyses were performed in a Micromeritics ASAP 2010 device by volumetric method. Samples (about 600 mg) were dried in He flow (30 mL/min) at 100 °C during 30 min, and reduced in H_2 (30 mL/min) at 500 °C during 2 h. A first outgas was performed at 500 °C during 60 min, followed by an outgas at 35 °C during 30 min. Total and reversible CO adsorption isotherms were measured at 35 °C and CO/Metal was calculated from irreversible CO uptake.

XPS analysis was carried out using an ESCALAB 250Xi spectrometer (Thermo Fisher Scientific) with monochromatic Al Kα X-rays (spot size of 900 μm). Surface charging of the electrically insulating materials was compensated using an integrated flood gun with approximate spot size of 900 μm. Survey spectra were obtained with a pass energy of 100 eV and region spectra (Ir4*f*, Al2*p*, Ni2*p*) using a pass energy of 25 eV. The base pressure of the analysis chamber was 7×10^{-10} mbar. Spectra were acquired, analyzed and peak fitted using the Avantage software with Lorentzian/Gaussian product function and a Shirley type background. Ir4*f* spectra were fitted with an energy constraint for $Ir4f_{5/2}$ within a 3 eV shift relative to the $Ir4f_{7/2}$ peak, an area ratio of 0.75:1, respectively, and a FWHM in the range 0.5–2.5 eV. Ni2*p* spectra were fitted with an energy constraint for $Ni2p_{3/2}$ within a 17.5 eV shift relative to the $Ni2p_{1/2}$ peak, an area ratio of 1:0.52, respectively, and a FWHM in the range 1.0–2.7 eV. The residual STD of the fitted spectra was around 0.9 for all catalysts. The binding energy (BE) calibration was done by adventitious carbon signal (C1*s* = 284.8 eV).

Morphological and nanostructural characterization of passivated catalysts were performed using a FEI Tecnai G2 Spirit Twin TEM with LaB6 filament operating at 120 kV.

Please cite this article in press as: A.J. Pamphile-Adrián, et al., Selective hydrogenolysis of glycerol over Ir-Ni bimetallic catalysts, Catal. Today (2016), http://dx.doi.org/10.1016/j.cattod.2016.07.026

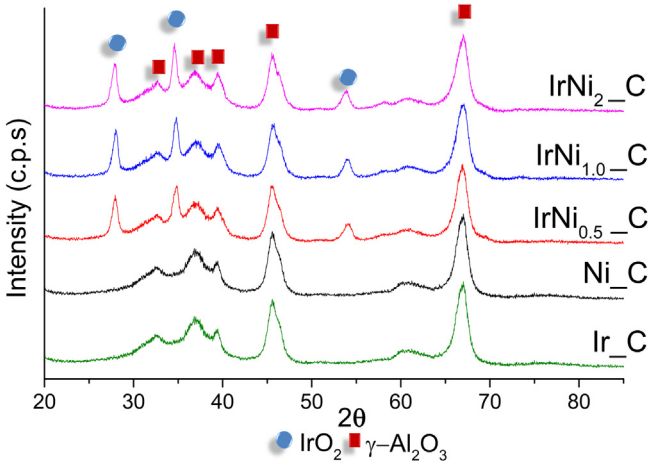

Fig. 1. XRD patterns for mono- and bimetallic calcined catalysts.

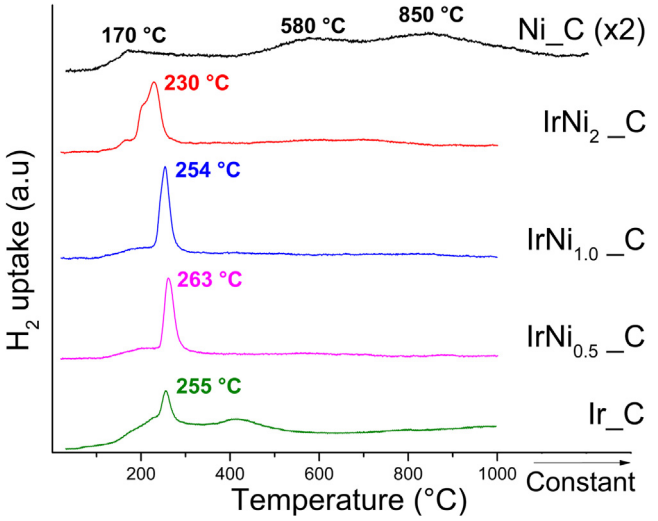

Fig. 2. Temperature programmed profiles for mono- and bimetallic calcined catalysts.

2.3. Glycerol hydrogenolysis

Glycerol hydrogenolysis was performed in a 300 mL autoclave reactor (Parr Instruments Co.). The reactor was initially loaded with 10.6 g of glycerol (Vetec Brasil), 40.6 g of deionized water and 1.6 g of catalyst (glycerol/Ir molar ratio of 714). The reactor was purged with a H_2 flow of 100 mL/min in order to remove air present in the system. After 10 min, H_2 pressure was raised to 360 psi, stirring speed was adjusted to 500 rpm and temperature was set to 200 °C. After the reaction time (12 h), the reactor was cooled to room temperature and the gas phase was collected and analyzed in a Micro-GC 490 (Agilent) equipped with three columns: M5A for permanent gases (H_2, O_2, N_2, CH_4 and CO), 5CB for hydrocarbons (C3-C6) and PPU for CO_2 and ethane. The liquid phase products were quantified in a GC–MS QP2010Plus (Shimadzu) equipped with a capillary column (Rtx-Wax). The products were identified using "GC–MS Solutions" software comparing with NIST05 and NIST05 s libraries. The identified products were 1,2 and 1,3 propanediol, propanol, ethylene glycol, isopropanol, ethanol, methanol and acetone. Initial TOF values were estimated for each catalyst from the initial reaction rate, assuming a first order reaction, and using CO chemisorption to estimate the number of surface metal sites. Product selectivity was calculated on carbon basis using the following equation:

$$\textit{Selectivity} \quad (\%) = \frac{j_i \times y_i}{\sum_i j_i \times y_i} \times 100$$

in which j_i is the number of carbons of product i and y_i is the molar fraction of product i.

For all reactions, gas phase products (CO, CO_2 and CH_4) were not considered for calculations, since their selectivities were negligible (<0.5%).

3. Results and discussion

3.1. Catalyst characterization

Fig. 1 presents X-ray diffractograms of prepared catalysts. In the case of calcined monometallic Ir and Ni catalysts, there were characteristic peaks of γ-Al_2O_3 (2θ = 32.7°, 36.9°, 39.5°, 45.6° and 67.0°. PDF N°066558). However, there were not any characteristic peaks of iridium or nickel species, probably due to low metal content, a high dispersion of metallic species on the support [26] or formation of an amorphous nickel aluminate, which could difficult the reduction of NiO species [27,28]. X-ray diffractograms of calcined $IrNi_x$ C bimetallic catalysts (Fig. 1) displayed characteristic peaks of IrO_2 at 27.6°, 34.5° and 53.7° (PDF N°431019), and characteristic peaks of nickel species were not observed. This result was not expected, since iridium content of bimetallic catalysts was the same as that of monometallic iridium catalyst (2 wt.%), but it could be explained by preferential sintering of iridium at calcination temperature of 500 °C [29]. On the other hand, X-ray diffractograms of non-calcined bimetallic catalysts (not shown) showed only γ-Al_2O_3 characteristic peaks, confirming that the agglomeration of iridium particles occurred due to the calcination step.

Table 1
Surface characterization of prepared catalysts by BET surface area, CO chemisorption and XPS analysis.

Catalyst	S_{BET} (m^2/g)	Irrev. CO uptake (μmol/g_{cat})	CO/M
γ-Al_2O_3	123	–	–
Ir_C	119	50.0	0.48
Ni_C	113	17.5	0.03
$IrNi_{0.5}$_C	108	10.0	0.06
$IrNi_{1.0}$_C	108	10.0	0.05
$IrNi_2$_C	108	11.0	0.04
Ir	–	19.3	0.19
$IrNi_{0.5}$	–	41.0	0.26
$IrNi_{1.0}$	–	58.4	0.28
$IrNi_2$	–	41.5	0.13

Temperature programed reduction profiles of prepared catalysts are shown in Fig. 2. The reduction profile of Ni_C catalyst presented three broad reduction peaks at 170, 580 and 850 °C. The first peak can be attributed to the reduction of well-dispersed NiO particles with weak interactions with support [30]. The second peak is due to reduction of NiO particles interacting with support and the last peak can be attributed to the reduction of nickel aluminate species ($NiAl_2O_4$) [31,32]. The TPR profile of monometallic iridium catalyst presented a main broad peak at 255 °C ascribed to the reduction of iridium oxide and iridium chloride species [16].

The TPR profiles of the bimetallic catalysts showed well-defined reduction peaks at 263 °C ($IrNi_{0.5}$_C), 254 °C ($IrNi_{1.0}$_C) and 230 °C ($IrNi_2$_C). In all cases, the peaks can be attributed to the simultaneous reduction of iridium and nickel oxide species [24]. This effect is produced by the strong interaction between both metals, which has been observed previously [24,25].

Table 1 depicts the results obtained for CO chemisorption on the studied catalysts. In all cases a linear adsorption was assumed (CO/M = 1, M = Ir or Ni) [33]. Iridium monometallic calcined cata-

Table 2
XPS results for monometallic Ir and Ni catalysts and bimetallic $IrNi_x$_C and $IrNi_x$_C_P series.

Catalyst	Ir4$f_{7/2}$				Ni2$p_{3/2}$		Ni/Ir[a]
	Ir^0 B.E. (eV)/At%	$Ir^{\delta+}$	IrO_2	$IrCl_x$	Ni^0	NiO	
Ir_C	–	–	61.3/60	63.7/40	–	–	
Ni_C	–	–	–	–	–	856.0/100	
$IrNi_{0.5}$_C	–	60.5/45	61.9/47	63.4/8	–	856.2/100	1.1
$IrNi_{1.0}$_C	–	60.4/27	61.2/49	62.6/24	–	855.5/100	0.7
$IrNi_2$_C	–	60.5/28	61.7/65	63.3/7	–	856.1/100	3.6
Ni_C_P	–	–	–	–	851.8/12	856.0/88	–
$IrNi_{0.5}$_C_P	59.7/54	60.6/39	62.7/7	–	–	–	–
$IrNi_{1.0}$_C_P	59.6/48	60.8/31	62.0/21	–	853.1/36	855.8/64	1.1
$IrNi_2$_C_P	59.7/68	60.8/30	62.6/2	–	852.9/19	855.4/81	5.1

[a] Ni/Ir calculated from At.% of Ir4*f* and Ni2*p* peaks in survey spectra.

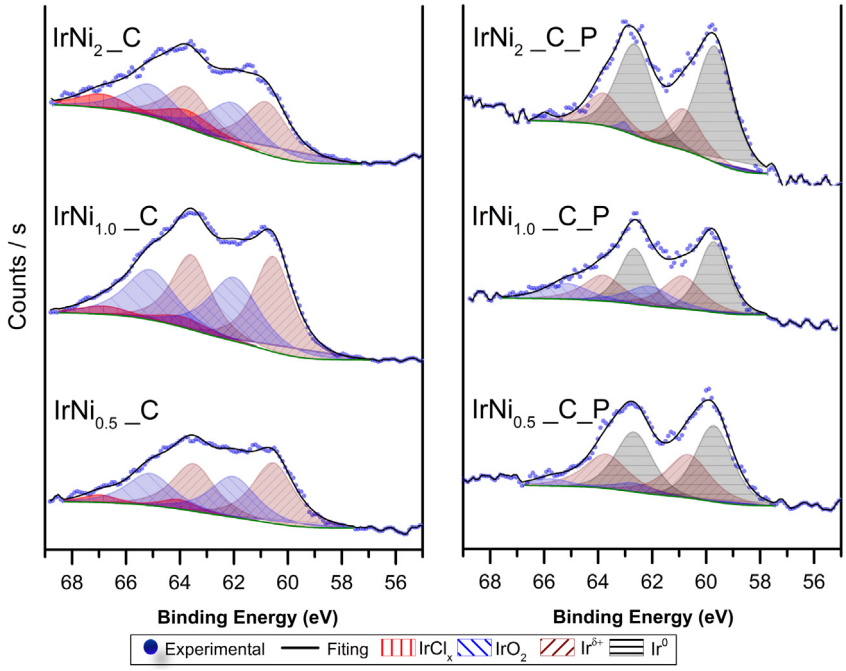

Fig. 3. XP spectra of the Ir4f spectral line of bimetallic $IrNi_x$_C and $IrNi_x$_C_P series.

lyst (Ir_C) presented the highest CO/M ratio (CO/Ir = 0.48), while monometallic Ni calcined catalyst presented the lowest CO/M ratio (CO/Ni = 0.05), about 10 times lower than for Ir_C catalyst. In general, for bimetallic calcined catalysts, the amount of adsorbed CO decreased with the addition of Ni. This behaviour was expected due to the low CO adsorption capacity presented by the monometallic Ni catalyst [34] and due to the sintering of Ir during calcination at 500 °C as observed by XRD. However, an increasing trend of CO/M ratio with the amount of Ni in the catalyst was observed. This trend could be attributed to Ir-Ni interactions that affect the adsorption of CO on the active sites [35]. Non-calcined series catalysts presented higher CO adsorption uptakes with the exception of monometallic Ir catalyst. For the latter, the low adsorption of CO can be related to the weak metal-support interactions due the absence of the calcination of the solid, which have a direct influence on the CO adsorption. In the case of the bimetallic non-calcined catalysts, there was an increase in the CO/M ratio, compared to calcined catalysts. This result is consistent with IrO_2 lines obtained in X-ray diffractograms and suggests the presence of large crystallites that could lead to a lower dispersion of the active phase on the support. Thus, the lower CO/M ratios obtained for the bimetallic Ir-Ni calcined catalysts is another evidence of sintering of the iridium surface particles caused by the elevated calcination temperature.

Table 2 depicts the results obtained for XPS analysis of monometallic iridium catalyst and bimetallic $IrNi_x$_C and $IrNi_x$_C_P series. For monometallic Ir_C catalyst, the deconvolution of Ir4*f* evidenced the presence of two iridium species. The doublets having lower binding energies (with Ir4$f_{7/2}$ at 61.3 eV) are attributed to surface IrO_2 [36–38], and the doublets with higher binding energies (with Ir4$f_{7/2}$ at 63.7 eV) can be attributed to the presence of surface iridium chloride species ($IrCl_3$ or $IrCl_4$) [39,40]. On the other hand, for bimetallic $IrNi_x$_C and $IrNi_x$_C_P series of catalysts, Fig. 3, the deconvolution of Ir4*f* peaks evidenced three iridium species on the surface of the catalysts. For $IrNi_x$_C series, besides the IrO_2 and $IrCl_x$ species, also observed in the monometallic catalyst, a third 4*f* doublet was found, with Ir4$f_{7/2}$ at 60.4 eV, for $IrNi_{1.0}$_C, and 60.5 eV, for $IrNi_{0.5}$_C and $IrNi_2$_C samples. This low binding energy doublet could be explained by the presence of an $Ir^{\delta+}$ species ($0 < \delta < +4$), product of the strong interaction between Ir and Ni, and can suggest that Ni is acting like an electronic density donor, leading Ir to an electron rich state, closer to metallic state. In the case of passivated catalysts, $IrNi_x$_C_P series, the presence of metallic iridium was confirmed, with Ir4$f_{7/2}$ at 59.6 eV, for IrNi_C_P, and 59.7 eV for $IrNi_{0.5}$_C_P and $IrNi_2$_C_P catalysts. It is important to note that this binding energy is 0.8 eV lower than that obtained for the $Ir^{\delta+}$ species founded for $IrNi_x$_C series. This difference confirms that $Ir^{\delta+}$ is an

Please cite this article in press as: A.J. Pamphile-Adrián, et al., Selective hydrogenolysis of glycerol over Ir-Ni bimetallic catalysts, Catal. Today (2016), http://dx.doi.org/10.1016/j.cattod.2016.07.026

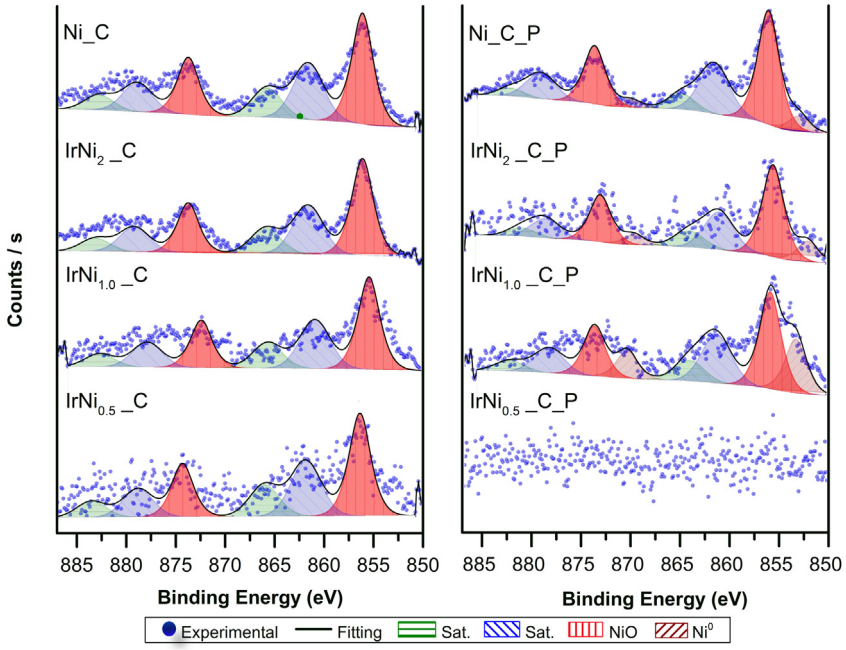

Fig. 4. XP spectra of the Ni2p spectral line of bimetallic $IrNi_x$_C and $IrNi_x$_C_P series.

Ir species with an electronic state between Ir^{4+} and Ir^0, produced by the strong interaction between Ir and Ni, as stated before. Additionally, for $IrNi_x$_C_P, surface IrO_2 was obtained, which could be formed in the passivation process of the samples.

Ni2*p* spectra for calcined monometallic Ni and bimetallic Ir-Ni catalysts are displayed in Fig. 4. It can be observed that for both calcined and passivated series of catalysts, lower content of Ni lead to less resolved peaks. This can be an evidence of the enrichment of the catalysts surface with Ir, turning peak fitting difficult. Spectra of passivated catalysts showed the presence of Ni^0 in low quantities, confirming the difficulty of the reduction of this series of catalysts. Additionally, the interaction between Ni and Ir was also confirmed by these spectra, were Ni^0 peaks were observed at 853.1 and 852.9 eV for IrNi_C_P and $IrNi_2$_C_P catalysts, respectively. These values are higher than binding energy values typically obtained for Ni^0 [17,41], which can be attributed to transference of electronic density from Ni to Ir, in agreement with the observations for Ir4*f* spectra.

3.2. Glycerol hydrogenolysis

Application of Weisz-Prater criterion indicated the catalytic results were free from internal mass transfer limitations. Table 3 displays the results of conversion and TOF for the glycerol hydrogenolysis over $IrNi_x$_C catalysts. For comparison, monometallic Ir and Ni calcined catalysts were also tested, and both catalysts presented low glycerol conversion (5.9% for Ir_C and 2.4% for Ni_C) and consequently low TOF values.

Bimetallic catalysts presented a significant increase in glycerol conversion compared to Ir and Ni monometallic catalysts. This increase in catalytic activity with the addition of Ni may be attributed to a synergic effect between both metals promoted by the modification of the iridium electronic state in the presence of nickel as observed in the XPS analysis, with a possible alloy formation after reduction. This result is in agreement with the results found by Jiang et al. [42] with a Pd-Ni catalyst in glycerol hydrogenolysis reaction. The authors prepared a bimetallic Pd-Ni catalyst (5 wt.% Pd), which catalytic activity and stability was much higher than that obtained for pure Ni using 1.0 g of catalyst in 100 mL of 20% glycerol solution, at 200 °C and 290 psi of H_2 during 12 h. Furthermore, Ueda et al. [43] have reported an increasing on activity and stability of a Ni/γ-Al_2O_3 catalyst for hydrogenolysis of glycerol by modification with a small amount of Pt, which was attributed to the formation of a Pt-Ni alloy.

In relation to product selectivity, Table 3, monometallic Ir catalyst exhibited a higher selectivity to 1,2-PDO than Ni monometallic catalyst, which presented the higher selectivity to propanol and acetol, which are produced by 1,2-PDO and glycerol dehydration, respectively [44]. In the case of the bimetallic catalyst, the selectivity to 1,2-PDO slightly decreased with the increase in the amount of Ni. However, it remained high (a minimum of 83.1% for $IrNi_2$_C catalyst). The opposite trend was observed for the selectivity to propanol, which slightly increased with the amount of added Ni. This result is consistent with that found for monometallic Ni catalyst, since the amount of propanol formed increased with the decrease of 1,2-PDO, which suggests that the addition of Ni promotes the dehydration of 1,2-PDO to form propanol.

Recycle tests of Ir-Ni calcined catalysts are displayed in Table 3, where a decrease between 3.7 and 5.7% in glycerol conversion was observed for all catalysts. It has been demonstrated that hot liquid water has a negative influence on the stability of γ-Al_2O_3, leading to a phase transition to bohemite [45,46]. However, Pt/Al_2O_3 catalysts prepared by impregnation of H_2PtCl_6 showed a resistance to this transition. The expected total bohemite fraction is about 0.6 for 1 wt% of Pt [45,46]. This behaviour could be expected to occur for impregnated Ir/Al_2O_3 catalysts. However, the results obtained for recycle catalysts showed that the phase transition of Al_2O_3 to bohemite is not relevant, since the decrease in activity would be more pronounced.

For the reactions performed with non-calcined catalysts different trends for catalyst activity were observed (Table 4). For $IrNi_{1.0}$ and $IrNi_2$, the values of glycerol conversion remained almost constant. However, a marked difference is observed for TOF values. In all cases, the TOF was about five times lower than that obtained for calcined catalysts. The higher TOF value was obtained for $IrNi_2$ catalyst, higher than that obtained for monometallic Ir catalyst, but lower than that obtained with $IrNi_2$_C catalyst.

Please cite this article in press as: A.J. Pamphile-Adrián, et al., Selective hydrogenolysis of glycerol over Ir-Ni bimetallic catalysts, Catal. Today (2016), http://dx.doi.org/10.1016/j.cattod.2016.07.026

Table 3
Glycerol conversion and product selectivity in glycerol hydrogenolysis reaction for calcined Ir, Ni and Ir- Ni catalysts.

Catalyst	Cycle	Conv. (%)	$(-r_A)_0 \times 10^{-7}$ (mol/s g_{cat})	TOF[a] $\times 10^{-2}$ (s^{-1})	Product Selectivity (%)					
					1,2-PDO	1,3-PDO	PrOH	EG	Acetol	Others
Ir_C	1	5.9	2.2	0.4	89.9	1.3	5.4	2.6	0.4	0.5
Ni_C	1	2.4	2.0	1.1	70.9	0.4	10.5	4.7	8.5	3.8
$IrNi_2$_C	1	24.3	4.7	4.3	83.1	2.2	7.0	5.8	0.1	1.8
	2	20.6	3.4	3.1	85.0	1.1	6.3	5.5	0.4	1.6
$IrNi_{1.0}$_C	1	21.2	4.2	4.2	87.2	1.8	4.3	4.7	0.2	1.8
	2	16.7	3.4	3.4	90.5	0.5	2.9	4.5	0.5	1.2
$IrNi_{0.5}$_C	1	19.5	3.9	3.9	88.9	2.1	3.2	4.5	0.2	1.2
	2	13.8	3.2	3.2	90.2	0.5	3.4	4.3	0.3	1.2

PDO = Propanediol; PrOH = Propanol; EG = Ethylene glycol; Others: Isopropanol, Ethanol, Methanol, Acetone. Reaction conditions: T = 200 °C; PH_2 = 360 psi; $m_{catalyst}$ = 1.6 g; 50 mL of 20% glycerol solution; $t_{reaction}$ = 12 h.
[a] Based on total liquid phase products normalized to the CO chemisorption of the fresh catalysts.

Table 4
Glycerol conversion and product selectivity in glycerol hydrogenolysis reaction for non-calcined Ir and Ir-Ni catalysts.

Catalyst	Conv. (%)	$(-r_A)_0 \times 10^{-7}$ (mol/s g_{cat})	TOF[a] $\times 10^{-2}$ (s^{-1})	Product Selectivity (%)					
				1,2-PDO	1,3-PDO	PrOH	EG	Acetol	Others
Ir	6.6	1.2	0.6	39.9	6.5	48.5	1.8	2.0	1.3
$IrNi_2$	22.3	5.4	1.3	80.8	1.7	10.9	5.0	0.0	1.6
$IrNi_{1.0}$	23.0	4.8	0.8	72.0	3.0	20.1	3.5	0.0	1.5
$IrNi_{0.5}$	15.7	3.1	0.8	77.8	2.8	16.4	2.3	0.1	0.8

Reaction conditions: T = 200 °C; PH_2 = 360 psi; $m_{catalyst}$ = 1.6 g; 50 mL of 20% glycerol solution; $t_{reaction}$ = 12 h. PDO = Propanediol; PrOH = Propanol; EG = Ethylene glycol; Others: Isopropanol, Ethanol, Methanol, Acetone.
[a] Based on total liquid phase products normalized to the CO chemisorption of the fresh catalysts.

Selectivity to 1,2-PDO also decreased for non-calcined catalysts. For monometallic Ir catalyst, selectivity to 1,2-PDO decreased about 50%, and a high amount of propanol was formed as a product of 1,2-PDO dehydration. Within non-calcined bimetallic catalysts, the higher selectivity to 1,2-PDO was obtained for $IrNi_2$ catalyst, however, it was lower than that obtained for $IrNi_2$_C catalyst. For all non-calcined bimetallic catalysts, a higher quantity of propanol was formed, compared to calcined catalysts, especially for $IrNi_{1.0}$ catalyst, which had the highest selectivity to propanol among the bimetallic catalysts.

All these observations suggest that the process of calcination is fundamental to determine the course of the glycerol hydrogenolysis reaction, in terms of activity and product selectivity, even for Ir monometallic catalyst. Spheroidal Ir-Ni particles (dark contrast) supported on γ-Al_2O_3 particles of irregular shapes are observed in multibeam TEM micrographs of passivated $IrNi_{1.0}$_C and $IrNi_{1.0}$ catalysts, presented in Fig. 5, where the differences in particles sizes are notorious.

$IrNi_{1.0}$ catalyst displayed small and well dispersed particles, between 1.9 and 3.5 nm. On the other hand, $IrNi_{1.0}$_C catalyst presented slightly larger particles, with sizes between 3.0 and 5.9 nm, suggesting that the non-calcined catalyst has more available active sites than the calcined catalyst, in agreement CO chemisorption analysis, where $IrNi_{1.0}$ catalyst showed the highest CO/M ratio. These observations are also in agreement with the results obtained for XRD analysis, where characteristic peaks of Ir species were obtained for $IrNi_{1.0}$ C catalysts, suggesting the presence of larger iridium particles. This results could be an evidence of the importance of the calcination process of the catalysts to obtain a strong Ir-Ni interaction that favors the glycerol conversion.

The effect produced by bimetallic catalysts in the course of the reaction can be due to a change of the number of atoms available for the reaction [47] or due to effects occasioned by electronic interactions between the components of bimetallic catalyst [35]. The notorious difference in the particle size of non-calcined and calcined catalysts may suggest that, besides electronic interactions, a structural effect could be responsible for the higher activity of calcined catalysts. However, apparently there is a controversy about metal size effect for glycerol hydrogenolysis reactions in the literature. Low metal dispersion (i.e. large metal particle size) has been reported as being favorable for this reaction [48,49]. On the other hand, in other catalytic systems smaller particles have yielded better activity [50,51]. Thus, a morphological effect caused by the agglomeration of Ir-Ni particles may also be acting as a favorable factor for the activity of bimetallic catalysts.

Electronic interactions between the components of bimetallic catalysts have a direct influence on the adsorption of the different reactants and products on the metallic surface. There are three main proposed mechanisms for glycerol hydrogenolysis that consist in dehydrogenation-dehydration-hydrogenation [52], direct hydrogenolysis [5] and dehydration-hydrogenation [44]. This last route involves the formation of acetol by glycerol dehydration as an intermediate that is subsequently hydrogenated to form 1,2-PDO. This mechanism has been reported to occur in the presence of acidic catalysts [53–56], which is the case of noble metal γ-Al_2O_3 supported catalysts [57].

The fact that acetol was obtained in low quantities in most of performed reactions, including those performed with Ir and Ni monometallic catalysts, could indicate that what determines the course of reaction is the glycerol adsorption on the catalyst surface, after which, acetol and subsequently 1,2-PDO are formed. Thus, the higher activity of bimetallic catalysts compared to the monometallic Ir and Ni catalysts is probably due to the effect produced by the electronic interactions between both metals. These interactions can be given in the form of chemical bonding, charge transferring or polarization effect [35]. In this case, the electronic transference from Ni to Ir that confers an electronic enrichment on Ir active sites was observed in XPS analysis.

In this context, it can be suggested that calcination process is fundamental to create a strong electronic interaction between Ir and Ni that provides active sites, which are more suitable for glycerol adsorption, and subsequently formation of products. Additionally, a structural effect could also be playing an important role, considering that the higher activity was obtained with the catalyst containing larger metal particles.

Please cite this article in press as: A.J. Pamphile-Adrián, et al., Selective hydrogenolysis of glycerol over Ir-Ni bimetallic catalysts, Catal. Today (2016), http://dx.doi.org/10.1016/j.cattod.2016.07.026

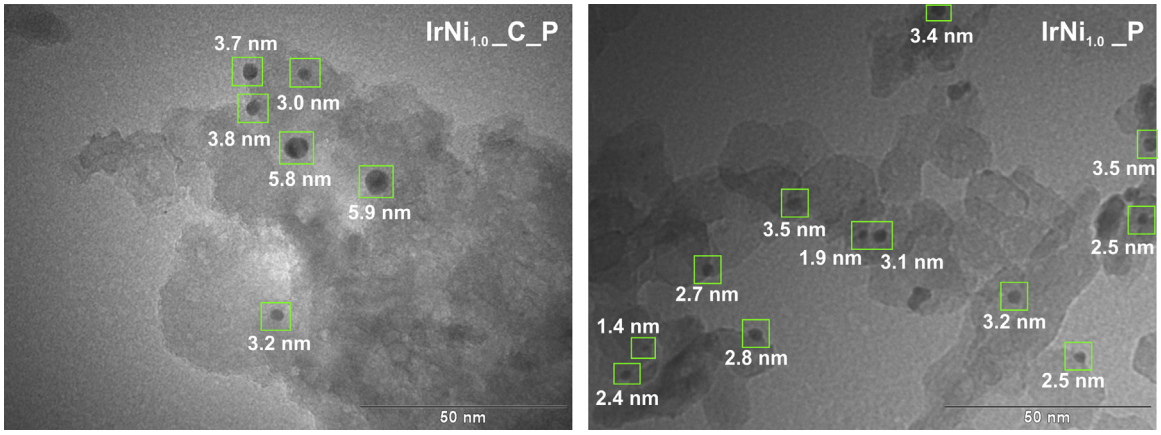

Fig. 5. Multi beam TEM micrographs of passivated $IrNi_{1.0}$_C and $IrNi_{1.0}$ catalysts.

4. Conclusions

The activity of calcined Ir-Ni bimetallic catalysts in glycerol hydrogenolysis was significantly higher than those obtained for monometallic Ir and Ni catalysts. Additionally, the selectivity to 1,2-PDO was as high as the one obtained for Ir catalyst. On the other hand, non-calcined bimetallic catalysts presented lower activity and selectivity to 1,2-PDO than calcined bimetallic catalysts, accompanied to a higher selectivity to propanol.

Ni-Ir interactions were evidenced in calcined bimetallic catalysts, and larger particles were observed by TEM analyses, compared to non-calcined bimetallic catalysts. Thus, the higher activity of calcined bimetallic catalysts can be explained in terms of a morphological and an electronic effect, both provided by the calcination process.

Acknowledgements

The authors gratefully acknowledge the funding from CAPES and CAPES/CNPq-IEL Nacional-Brasil (scholarships for P.P.F.R. and A.J.P.), FAPERJ and CNPq.

References

[1] E.M. Visser, D.O. Filho, M.A. Martins, B.L. Steward, Biomass Bioenergy 35 (2011) 489–494.
[2] D.E. Leiva-Candia, S. Tsakona, N. Kopsahelis, I.L. García, S. Papanikolaou, M.P. Dorado, A.A. Koutinas, Bioresour. Technol. 190 (2015) 57–65.
[3] Y. Nakagawa, Y. Shinmi, S. Koso, K. Tomishige, J. Catal. 272 (2010) 191–194.
[4] T. Kurosaka, H. Maruyama, I. Naribayashi, Y. Sasaki, Catal. Commun. 9 (2008) 1360–1363.
[5] Y. Nakagawa, M. Tamura, K. Tomishige, J. Mater. Chem. A 2 (2014) 6688–6702.
[6] Y. Nakagawa, K. Tomishige, Catal. Sci. Technol. 1 (2011) 179–190.
[7] Y. Amada, Y. Shinmi, S. Koso, T. Kubota, Y. Nakagawa, K. Tomishige, Appl. Catal. B: Environ. 105 (2011) 117–127.
[8] Y. Nakagawa, X. Ning, Y. Amada, K. Tomishige, Appl. Catal. A: Gen. 433–434 (2012) 128–134.
[9] Y. Amada, H. Watanabe, M. Tamura, Y. Nakagawa, K. Okumura, K. Tomishige, J. Phys. Chem. C 116 (2012) 23503–23514.
[10] M. Tamura, Y. Amada, S. Liu, Z. Yuan, Y. Nakagawa, K. Tomishige, J. Mol. Catal. A: Chem. 388–389 (2014) 177–187.
[11] Y. Nakagawa, K. Mori, K. Chen, Y. Amada, M. Tamura, K. Tomishige, Appl. Catal. A: Gen. 468 (2013) 418–425.
[12] K. Tomishige, M. Tamura, Y. Nakagawa, Chem. Rec. 14 (2014) 1041–1054.
[13] C. Deng, L. Leng, X. Duan, J. Zhou, X. Zhou, W. Yuan, J. Mol. Catal. A: Chem. 410 (2015) 81–88.
[14] C. Deng, X. Duan, J. Zhou, X. Zhou, W. Yuan, S.L. Scott, Catal. Sci. Technol. 5 (2015) 1540–1547.
[15] W. Luo, y. Lyu, L. Gong, H. Du, T. Wang, Y. Ding, RSC Adv. 6 (2016) 13600–13608.
[16] A.J. Pamphile-Adrián, P.P. Florez-Rodriguez, F.B. Passos, J. Braz. Chem. Soc. 27 (2016) 958–966.
[17] P.P. Florez-Rodriguez, A.J. Pamphile-Adrián, F.B. Passos, Catal. Today 237 (2014) 38–46.
[18] A. Iriondo, J.F. Cambra, V.L. Barrio, M.B. Guemez, P.L. Arias, M.C. Sanchez-Sanchez, R.M. Navarro, J.L.G. Fierro, Appl. Catal. B: Environ. 106 (2011) 83–93.
[19] B.C. Miranda, R.J. Chimentao, J.B.O. Santos, F. Gispert-Guirado, J. Llorca, F. Medina, F.L. Bonillo, J.E. Sueiras, Appl. Catal. B: Environ. 147 (2014) 464–480.
[20] K. Li, M. Jiao, Y. Wang, Z. Wu, Surf. Sci. 617 (2013) 149–155.
[21] L. He, Y. Huang, X.Y. Liu, L. Li, A. Wang, X. Wang, C.-Y. Mou, T. Zhang, Appl. Catal. B: Environ. 147 (2014) 779–788.
[22] K. Nakagawa, N. Ikenaga, Y. Teng, T. Kobayashi, T. Suzuki, Appl. Catal. A: Gen. 180 (1999) 183–193.
[23] W. Lin, H. Cheng, L. He, Y. Yu, F. Zhao, J. Catal. 303 (2013) 110–116.
[24] X. Han, W. Chu, P. Ni, S.-z. Luo, T. Zhang, J. Fuel Chem. Technol. 35 (2007) 691–695.
[25] S. Dokjampa, T. Rirksomboon, D.T.M. Phuong, D.E. Resasco, J. Mol. Catal. A: Chem. 274 (2007) 231–240.
[26] H. Tian, T. Zhang, X. Sun, D. Liang, L. Lin, Appl. Catal. A: Gen. 210 (2001) 55–62.
[27] A.L. Alberton, M.M.V.M. Souza, M. Schmal, Catal. Today 123 (2007) 257–264.
[28] S. Jin, Z. Xiao, C. Li, X. Chen, L. Wang, J. Xing, W. Li, C. Liang, Catal. Today 234 (2014) 125–132.
[29] R.M.J. Fiedorow, B.S. Chahar, S.E. Wanke, J. Catal. 51 (1978) 193–202.
[30] C. Li, Y.-W. Chen, Thermochim. Acta 256 (1995) 457–465.
[31] J.M. Rynkowski, T. Paryjczak, M. Lenik, Appl. Catal. A: Gen. 106 (1993) 73–82.
[32] M.C. Sánchez-Sánchez, R.M. Navarro, J.L.G. Fierro, Int. J. Hydrogen Energy 32 (2007) 1462–1471.
[33] G.B. McVicker, R.T.K. Baker, R.L. Garten, E.L. Kugler, J. Catal. 65 (1980) 207–220.
[34] C.H. Bartholomew, R.B. Pannell, J. Catal. 65 (1980) 390–401.
[35] J.A. Rodriguez, D.W. Goodman, J. Phys. Chem. 95 (1991) 4196–4206.
[36] M. Peuckert, Surf. Sci. 144 (1984) 451–464.
[37] L. Atanasoska, R. Atanasoski, S. Trasatti, Vacuum 40 (1990) 91–94.
[38] J. Riga, C. Tenret-Noël, J.J. Pireaux, R. Caudano, J.J. Verbist, Y. Gobillon, Phys. Scr. 16 (1977) 351.
[39] B. Folkesson, Acta Chem. Scand. 27 (1973) 287–302.
[40] Y.I. Kim, W.E. Hatfield, Inorg. Chim. Acta 188 (1991) 15–24.
[41] M.L. Barbelli, M.D. Mizrahi, F. Pompeo, G.F. Santori, N.N. Nichio, J.M. Ramallo-Lopez, J. Phys. Chem. C 118 (2014) 23645–23653.
[42] T. Jiang, Q. Huai, T. Geng, W. Ying, T. Xiao, F. Cao, Biomass Bioenergy 78 (2015) 71–79.
[43] N. Ueda, Y. Nakagawa, K. Tomishige, Chem. Lett. 39 (2010) 506–507.
[44] I. Gandarias, P.L. Arias, J. Requies, M.B. Guemez, J.L.G. Fierro, Appl. Catal. B: Environ. 97 (2010) 248–256.
[45] R.M. Ravenelle, J.R. Copeland, W.-G. Kim, J.C. Crittenden, C. Sievers, ACS Catal. 1 (2011) 552–561.
[46] R.M. Ravenelle, F.Z. Diallo, J.C. Crittenden, C. Sievers, ChemCatChem 4 (2012) 492–494.
[47] L. Guczi, Catal. Today 101 (2005) 53–64.
[48] Y. Li, L. Ma, H. Liu, D. He, Chin. J. Catal. 35 (2014) 677–683.
[49] B.K. Kwak, D.S. Park, Y.S. Yun, J. Yi, Catal. Commun. 24 (2012) 90–95.
[50] V. Montes, M. Checa, A. Marinas, M. Boutonnet, J.M. Marinas, F.J. Urbano, S. Jaras, C. Pinel, Catal. Today 223 (2014) 129–137.
[51] J. Feng, H.Y. Fu, J.B. Wang, R.X. Li, H. Chen, X.J. Li, Catal. Commun. 9 (2008) 1458–1464.
[52] E.P. Maris, R.J. Davis, J. Catal. 249 (2007) 328–337.
[53] Y. Kusunoki, T. Miyazawa, K. Kunimori, K. Tomishige, Catal. Commun. 6 (2005) 645–649.
[54] T. Miyazawa, S. Koso, K. Kunimori, K. Tomishige, Appl. Catal. A: Gen. 329 (2007) 30–35.
[55] T. Miyazawa, Y. Kusunoki, K. Kunimori, K. Tomishige, J. Catal. 240 (2006) 213–221.
[56] T. Miyazawa, S. Koso, K. Kunimori, K. Tomishige, Appl. Catal. A: Gen. 318 (2007) 244–251.
[57] S.N. Delgado, D. Yap, L. Vivier, C. Especel, J. Mol. Catal. A: Chem. 367 (2013) 89–98.

Please cite this article in press as: A.J. Pamphile-Adrián, et al., Selective hydrogenolysis of glycerol over Ir-Ni bimetallic catalysts, Catal. Today (2016), http://dx.doi.org/10.1016/j.cattod.2016.07.026